Plasma Doppler spectroscopy and tomography using spatial-multiplex coherence imaging techniques

John Howard

C Michael[1], F. Glass[1], J. Chung[2]

[1]Plasma Research Laboratory,
Australian National University

[2]Max Planck Institute for Plasma Physics
Greifswald, Germany

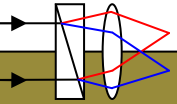

Outline

- Doppler tomography of inhomogeneous radiating media
- Coherence imaging for Doppler spectroscopy
  - Principles and methods
  - 1-D coherence camera results on H-1 heliac
  - 2-D Modulated Coherence Imaging systems – WEGA stellarator
- Static quadrature coherence imaging
  - 2-D static coherence camera results on H-1 heliac
- Other applications
  - Intensity ratios, isotope abundances etc.
  - Polarization spectroscopy (MSE, Zeeman)
  - More complex spectra - hybrid spatio-temporal multiplex systems
  - Broadband: Thermography, Thomson scattering

H-1NF accommodates imaging diagnostic systems

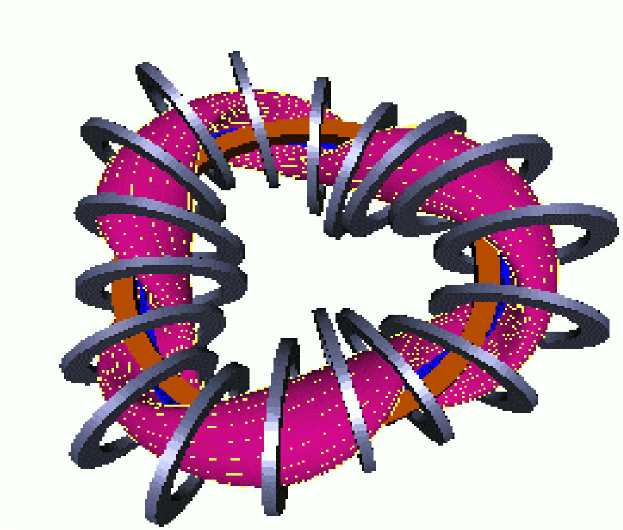

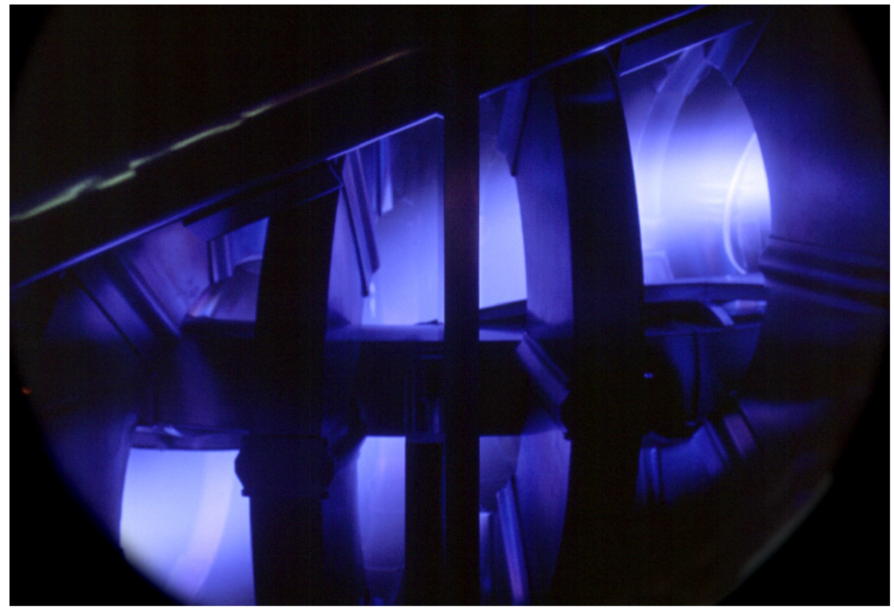

H-1NF: 3 period helical axis stellarator

Flexible magnetic configuration, rotational transform 1.-1.5, B 0-1T

7MHz, 80kW rf

28GHz 200kW ECH (2nd harmonic @0.5T)

Operations: Low field 0.1T Ar, helicon type discharges

Moderate field 0.5T ECH H/D/He

3.5 academic staff, 5-10 PhD + visitors + undergrads

Can Doppler spectroscopy give *f(r,v)* ?

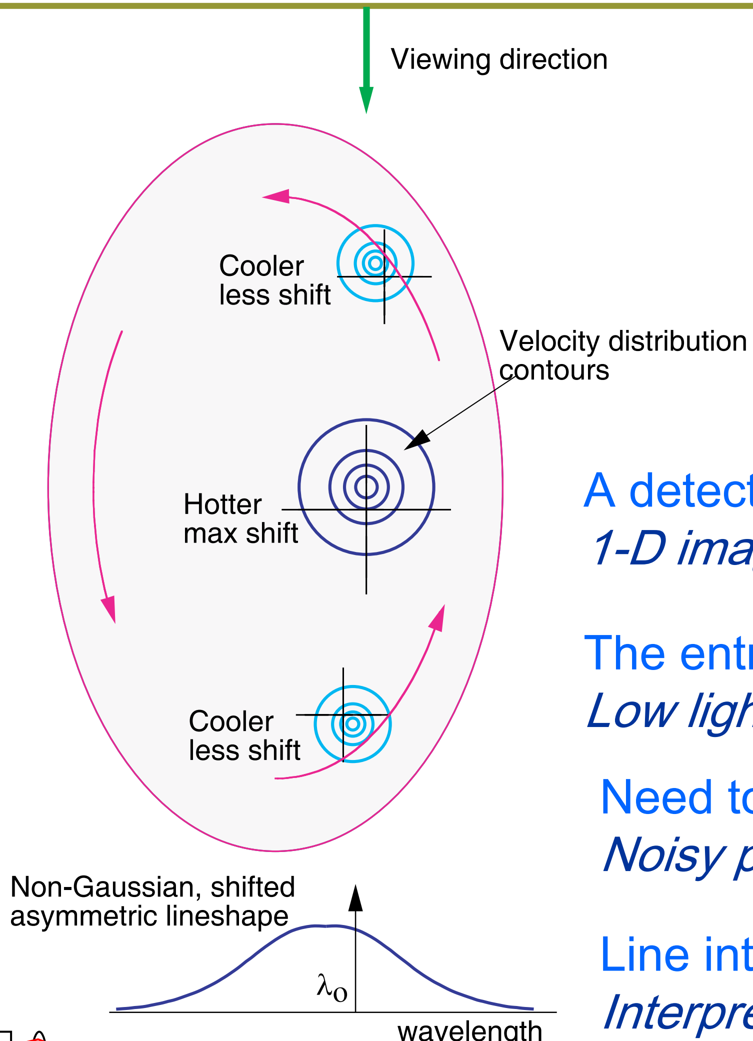

A standard frequency-domain spectrometer must measure the full spectral line profile in many different directions to unfold the intensity weighted contributions.

A detector array is needed to measure the spectrum width.
1-D imaging requires a 2-D array

The entrance aperture is a narrow slit.
Low light flux, poor time resolution

Need to unfold the instrument profile
Noisy process, uncertainties

Line integral of inhomogeneous medium
Interpretation difficult. Tomography?

How does Doppler effect reveal the inhomogeneous distribution function $f(r,\upsilon)$?

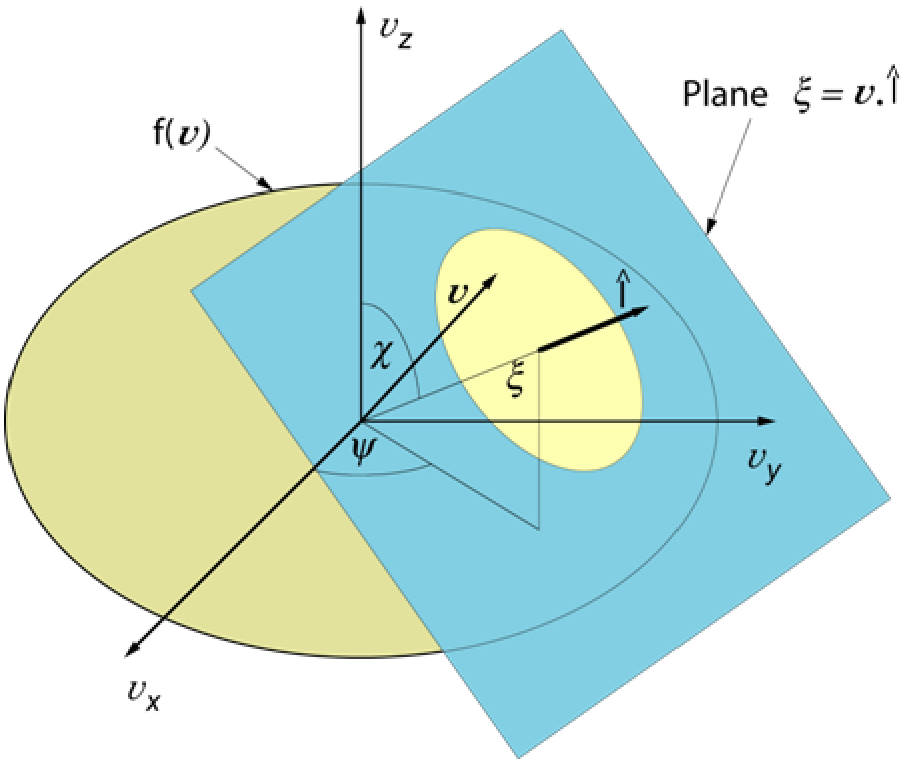

By the Doppler effect, particles g in f having velocity component υ in the direction $\boldsymbol{l}$ radiate at normalized frequency $\xi = \upsilon/c = (\nu - \nu_0)/\nu_0$:

3-d Radon transform

$$g(\boldsymbol{r}, \xi; \hat{\boldsymbol{l}}) = \int f(\boldsymbol{r}, \boldsymbol{v})\, \delta(\xi - \boldsymbol{v}.\hat{\boldsymbol{l}})\, \mathrm{d}\boldsymbol{v}.$$

When the medium is inhomogeneous ...

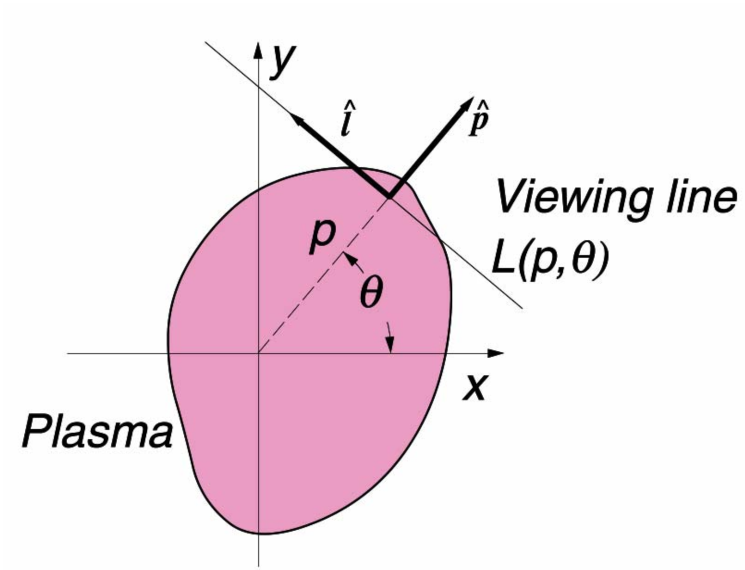

Another 2-d Radon transform

We measure the optical emission spectrum:

$$\begin{aligned} e(\xi;\hat{\boldsymbol{l}}) &= \int g(\boldsymbol{r},\xi;\hat{\boldsymbol{l}})\,\delta(p-\boldsymbol{r}.\hat{\boldsymbol{p}})\,\mathrm{d}\boldsymbol{r} \\ &\equiv \int_L g(\boldsymbol{r},\xi;\hat{\boldsymbol{l}})\,\mathrm{d}l. \end{aligned}$$

normalized frequency
$\xi = \upsilon/c = (\nu-\nu_0)/\nu_0$

Projection theorem for Doppler spectroscopy

Take Fourier transform of optical emission spectrum:

$$e(\xi;\hat{\boldsymbol{l}}) = \int \mathrm{d}\boldsymbol{r}\,\delta(p-\boldsymbol{r}.\hat{\boldsymbol{p}}) \int \mathrm{d}\boldsymbol{v}\,\delta(\xi-\boldsymbol{v}.\hat{\boldsymbol{l}})\, f(\boldsymbol{r},\boldsymbol{v})$$

$(\xi = \upsilon/c = (\nu-\nu_0)/\nu_0)$

$$\Rightarrow \quad E(k,\phi;\hat{\boldsymbol{l}}) = F(k\hat{\boldsymbol{p}},\phi\hat{\boldsymbol{l}})$$

Cannot recover 4-d function $f(x,y,\upsilon_x\ \upsilon_y)$ from 3-d measurement $E(k,\phi,\boldsymbol{l})$

The tomography problem is invertible when f is a locally drifting isotropic distribution.

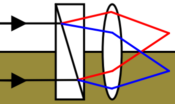

Interferometers measure the Fourier transform of the spectral lineshape: $f(r,\upsilon)$

$S = \mu_0[1 +/- \gamma(\phi)]$

$\gamma(\phi, l)$ is the complex coherence (FT of spectral lineshape)

μ_0 is the spectrally integrated emission intensity

ϕ is the optical delay

The fringe visibility is given by $\zeta = |\gamma(\phi, l)|$

The fringe phase is given by by $\mathrm{atan}(\gamma)$

Drifting Local Thermal Equilibrium

The Fourier transform separates the local drift from the body of *f*:

$f(r, \upsilon - \upsilon_D) \longrightarrow \exp(i\phi\, \upsilon_D . l/c)\, F_0(r, \phi)$

The fringe visibility gives the even part of isotropic *f(v)* (temperature):

$$\gamma(\phi; \hat{\boldsymbol{l}}) \,| = \frac{1}{\mu_0} \int_L I_0(\boldsymbol{r}) \, \exp\left[-T_S(\boldsymbol{r})/T_C\right] \, \mathrm{d}l$$

Scalar line integral

The change in interferometer phase gives line integrated Doppler shift:

$$\frac{\delta\phi}{\phi} = \frac{1}{\mu_0 \, |\gamma|} \int_L F_0(\boldsymbol{r}, \phi) \, \boldsymbol{V}(\boldsymbol{r}) . \mathrm{d}\boldsymbol{l}$$

Vector field integral

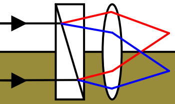

Tomography of vector fields

A measurement can be sensitive to a vector field component either along or transverse to the line-of-sight:

- Longitudinal ⇨ vorticity
- Transverse ⇨ sources and sinks

For fields with cylindrical (or toroidal) symmetry:

- Longitudinal ⇨ z-component of vector potential (solenoidal)
- Transverse ⇨ scalar potential (irrotational)

What is coherence imaging?

- When spectral information content is small (M unknowns), it suffices to image the optical coherence (interferogram) of the light emission at a small number (N>M) of optical delays.
- Why measure optical coherence?
  - Interferometers have high throughput (no slit)
  - Robust alignment, birefringent optics
  - time/space multiplex methods – 2D imaging

Coherence imaging using a modulated fixed delay polarization interferometer

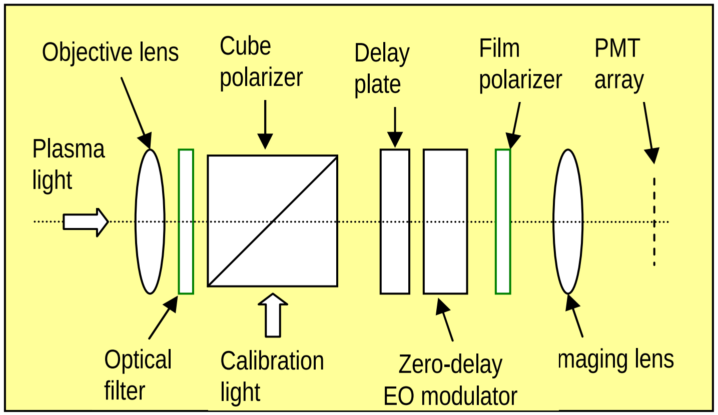

Single channel system:
"MOSS" - Modulated Solid Spectrometer

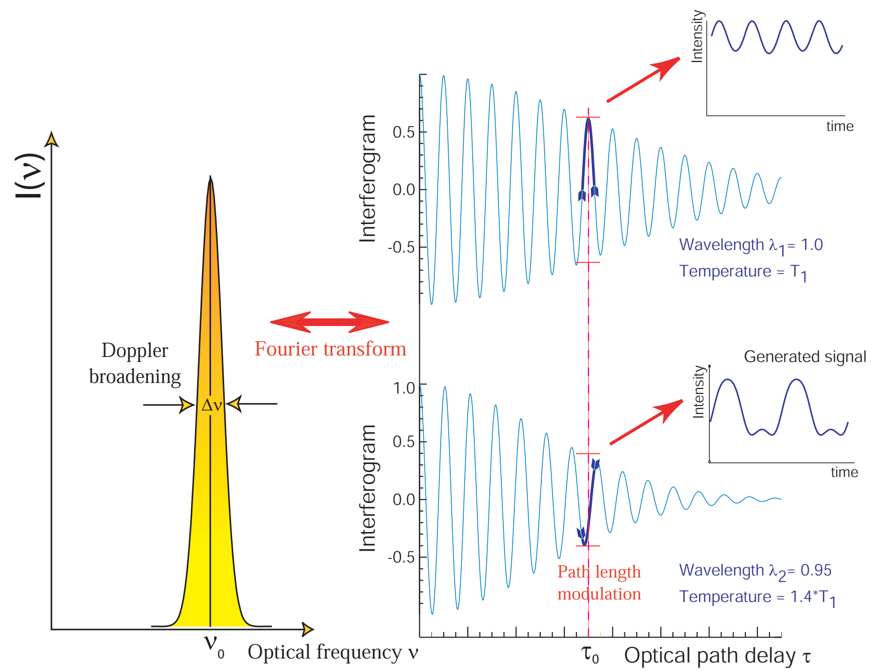

Multi-channel systems:
Coherence Imaging System (CIS)
Images the amplitude and phase of interferogram at one or more fixed delays
Both temporal modulation and spatial multiplex (static) encoding methods

Waveplate delay fixes targeted optical "coherence length".
Large delay, long coherence length, narrow linewidth => colder
Waveplate delay defines the instrument "characteristic temperature" T_c

1-D Coherence imaging camera on H-1

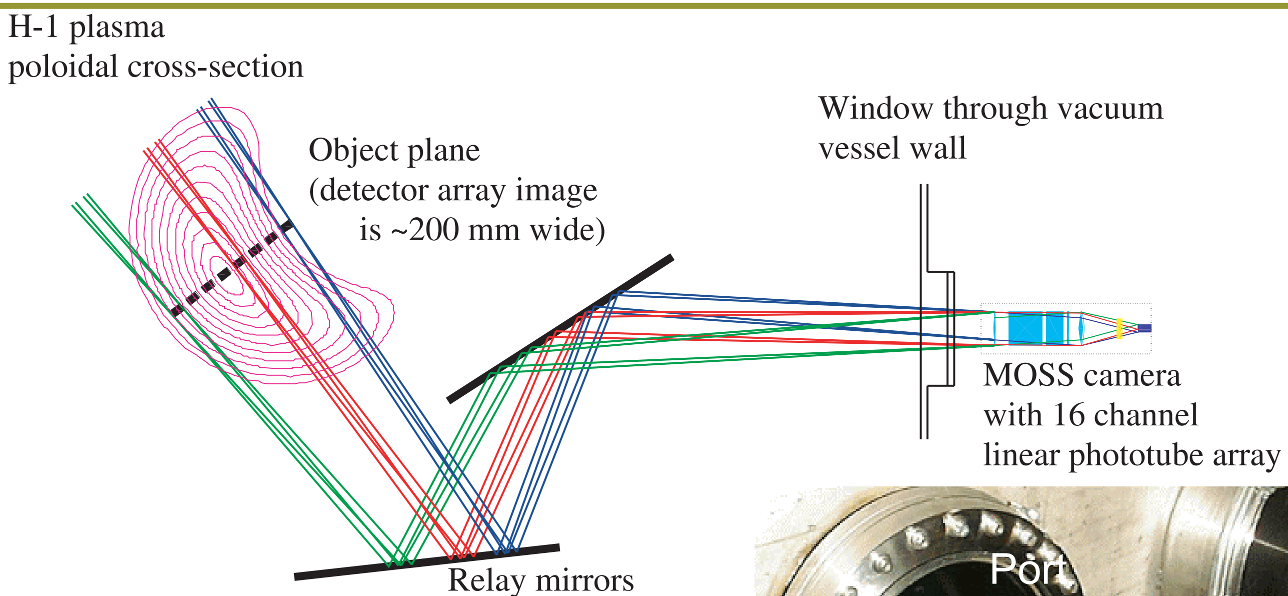

Field of view ~30^o
16 or 32 channels, 1-2cm resolution
50kHz modulation frequency

Camera and calibration optics

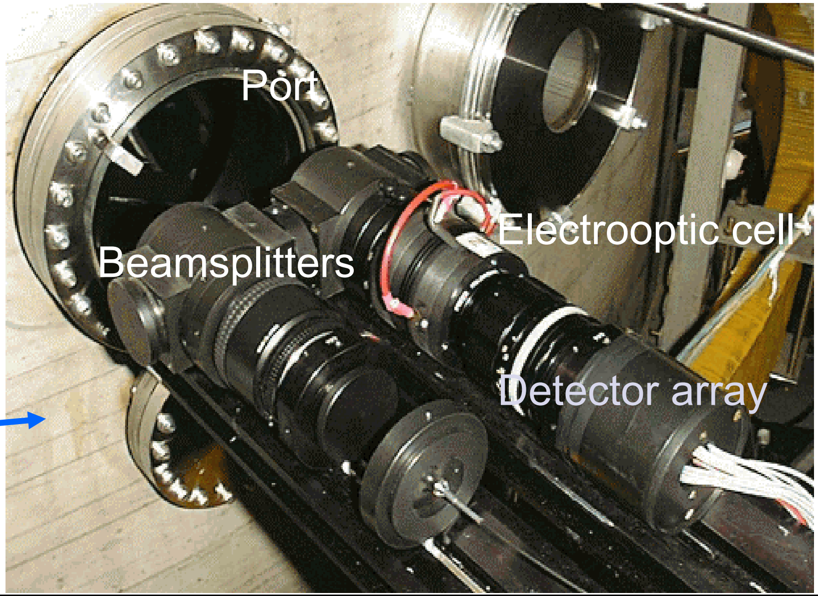

Integrated PMT/amplifier array detector units

Front view, including lens

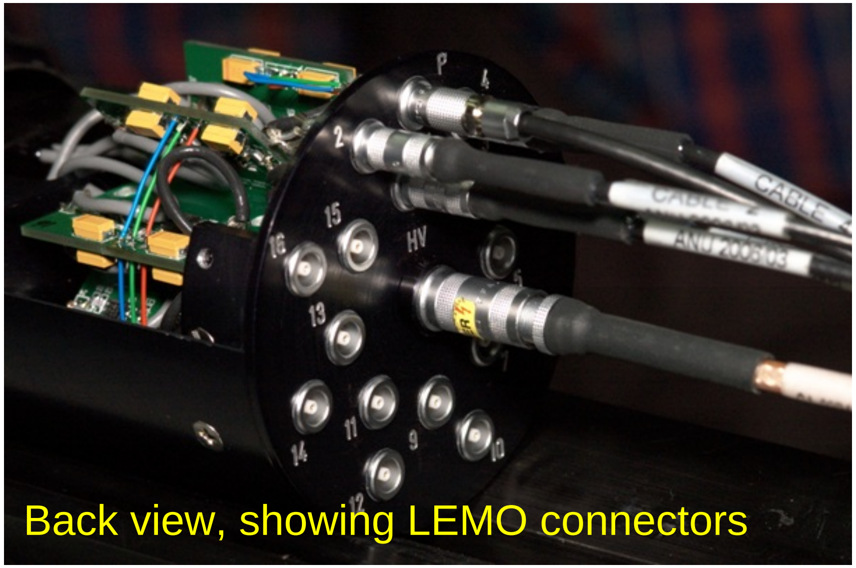

Back view, showing LEMO connectors

PMT (multi-anode) 16 channel detector array (Hamamatsu) with integrated amplifiers with magnetic shielding (75mm diameter).

These units couple directly to the front end modulated interferometer via standard F-mount lens

Imaging systems allow spatially-resolved dynamical studies

Outside

Inside

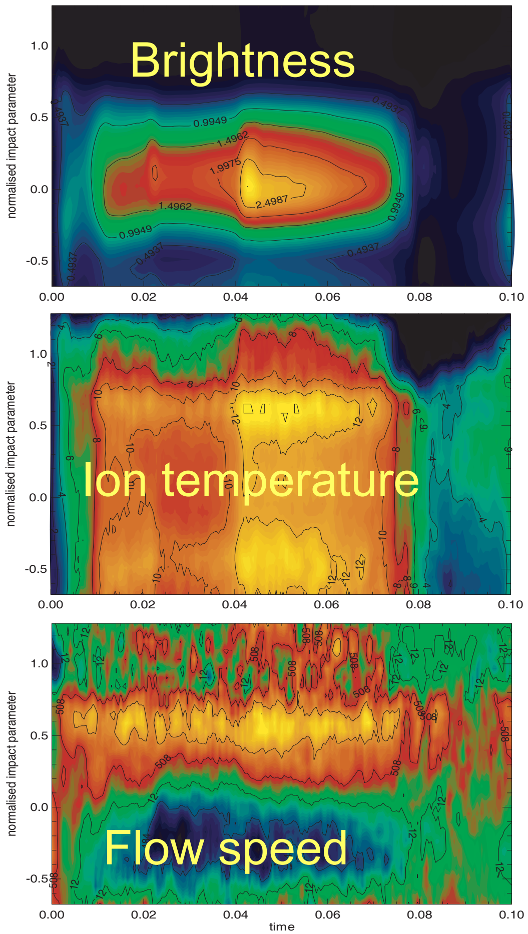

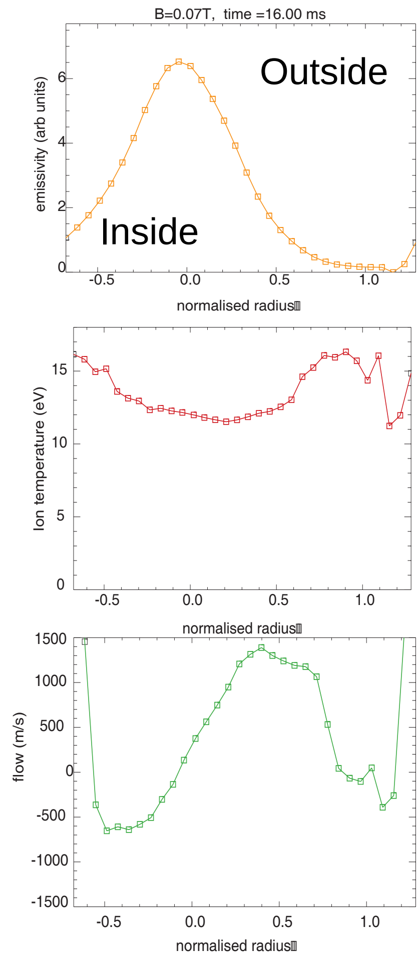

Brightness

Temperature

Non thermal features and higher temperatures in plasma edge

Flow speed

Sheared rigid rotation

Profiles during power ramp experiments

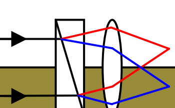

Coherence and spectral measurements agree

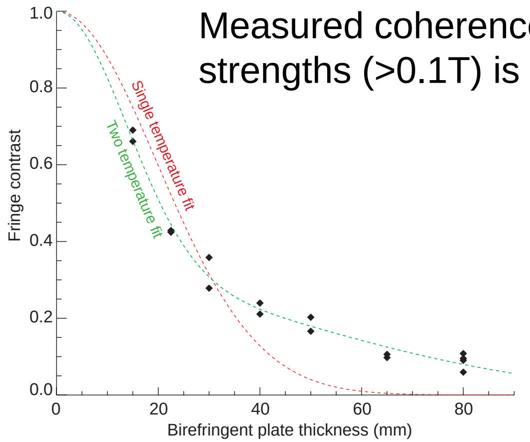

Measured coherence at higher field strengths (>0.1T) is non-Gaussian

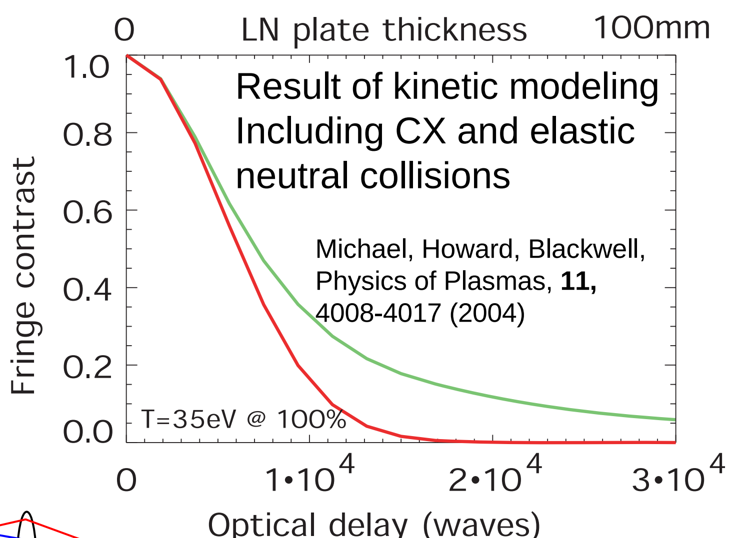

Result of kinetic modeling Including CX and elastic neutral collisions

Michael, Howard, Blackwell, Physics of Plasmas, **11,** 4008-4017 (2004)

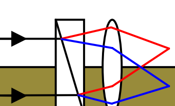

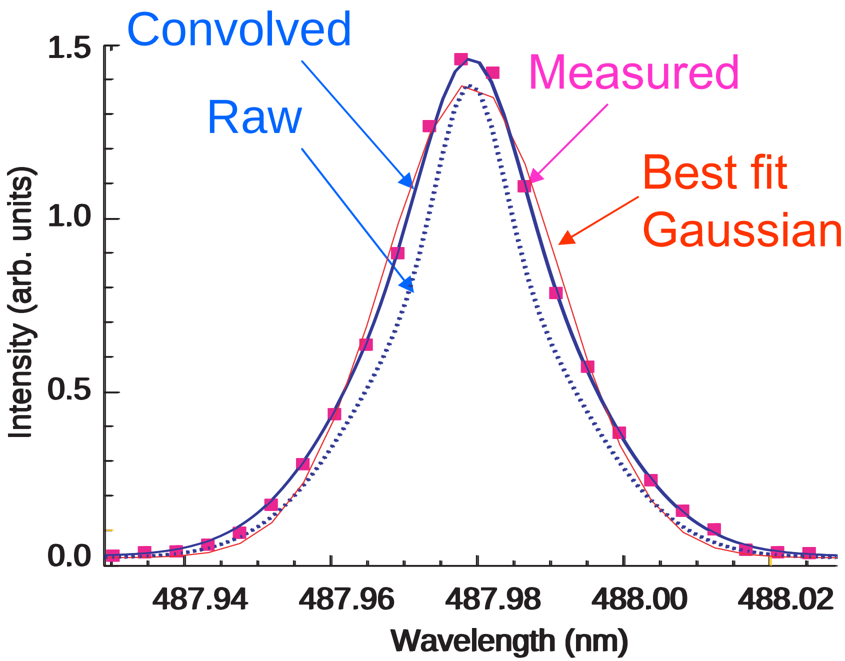

Strong coupling with Ar neutral background distorts ion *f(v)*

Next step: fast CCD camera for 2-D imaging

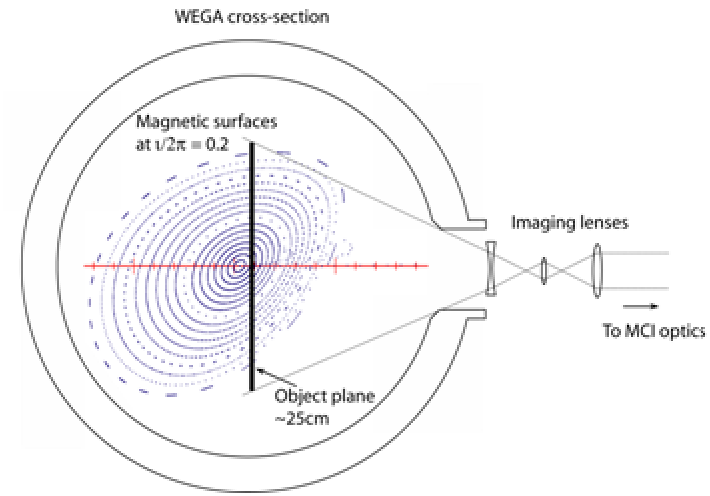

The IPP-WEGA camera:

Thermally compensated lithium tantalate electrooptic modulator

- Lithium niobate delay plates
- LabVIEW/MDSplus control software
- Cooled CCD, 12 bit camera,
- max 70Hz frame rate

Ion temperature animation
(WEGA ECH power step, HeII 468nm)

Systems for RFX, IPP, KSTAR

Comparison of coherence imaging system with 1-D Echelle

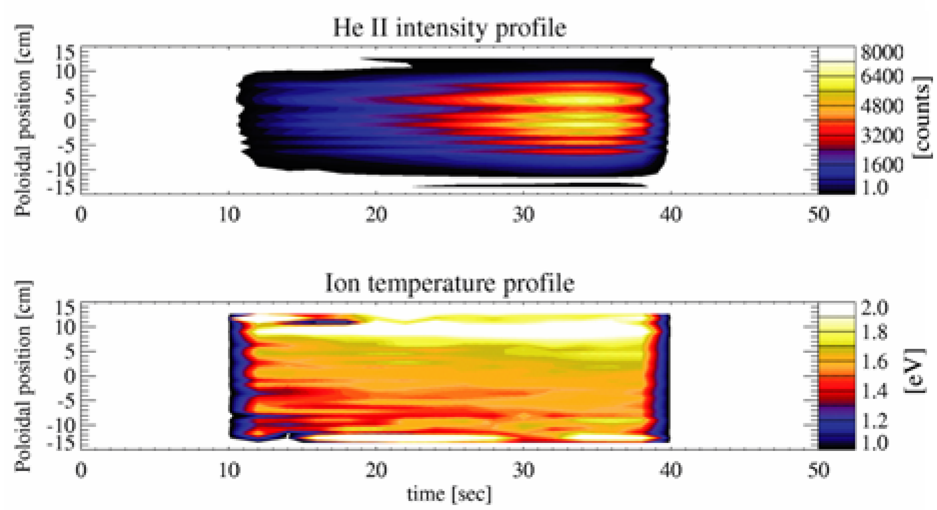

Echelle
16 channel optical fibre array
1-D slice, 10ms integration

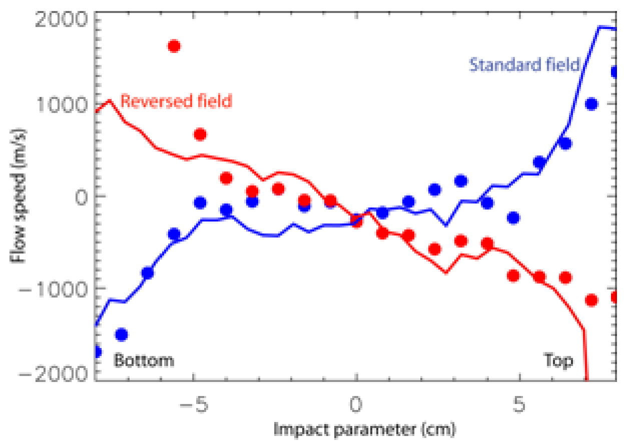

Echelle (dots)
Coherence imaging (lines)
Blue: standard field direction
Red: reversed field direction

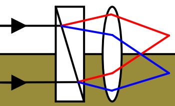

ANU

Spatial multiplex quadrature coherence imaging

Time multiplex methods cannot resolve fast phenomena: Spatial multiplex (no modulation) - Brightness, contrast and phase in a single snapshot

- High throughput - in principle 100% light efficient
- Spatial multiplex
  - no modulation
  - instantaneous information
  - High speed/synchronous Doppler imaging of breakdown phenomena, transients, combustions etc
- Passive components - extension to UV (>200nm)
- Can be integrated with step modulator for study of more complex scenes.

Static quadrature coherence imager

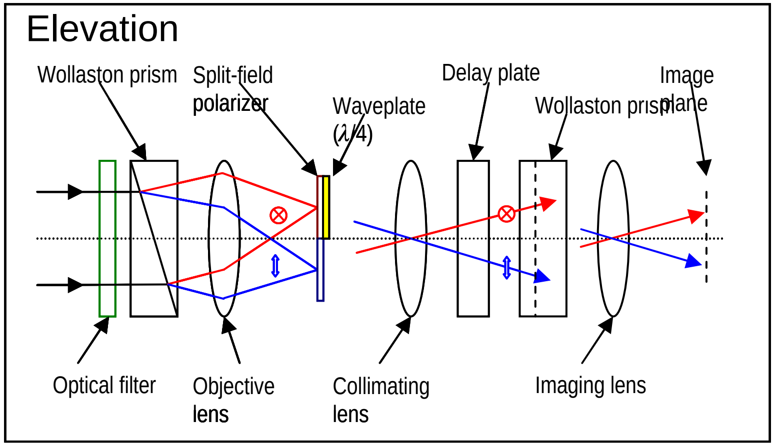

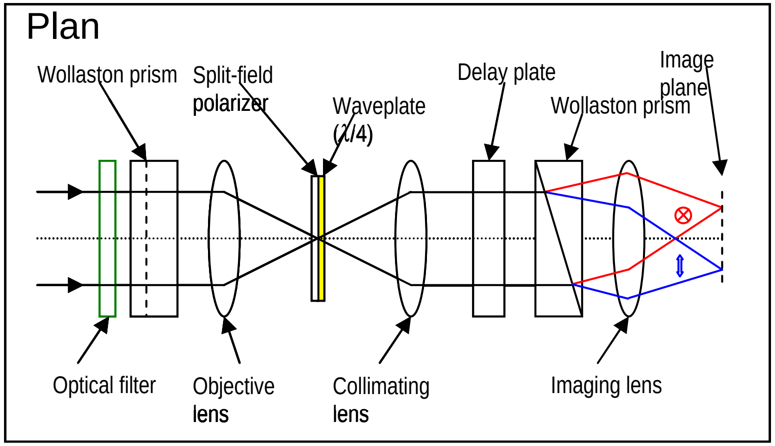

Front end Wollaston/mask produces dual orthogonally polarized images of source.

A polarizer isolates the images and a quarter waveplate produces 90º phase shift in one image

These are angularly multiplexed through the fixed-delay polarization interferometer

A final Wollaston produces antiphase interferograms for each of the source images

The four images generate a quadrature sampling of the interferogram about a fixed delay

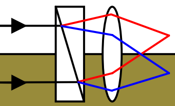

Static quadrature coherence imager

Quadrature images

Complementary images

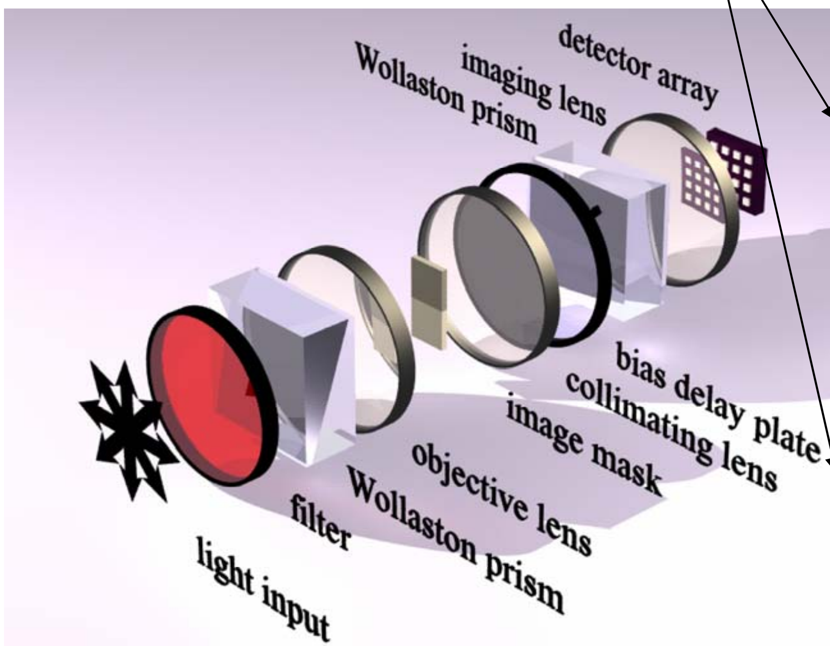

3-d layout for quad imager

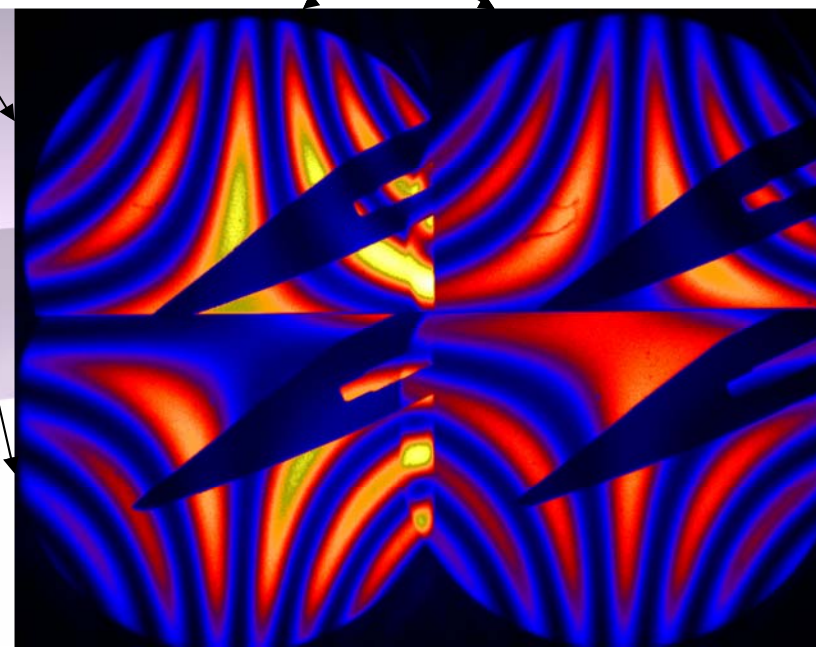

Scalpel blade image against backdrop of monochromatic birefringent-plate interference fringes

Hardware layout of Quadrature Coherence Imaging System for KSTAR

Camera

Back Wollaston

EO modulator (for calibration)

Front Wollaston

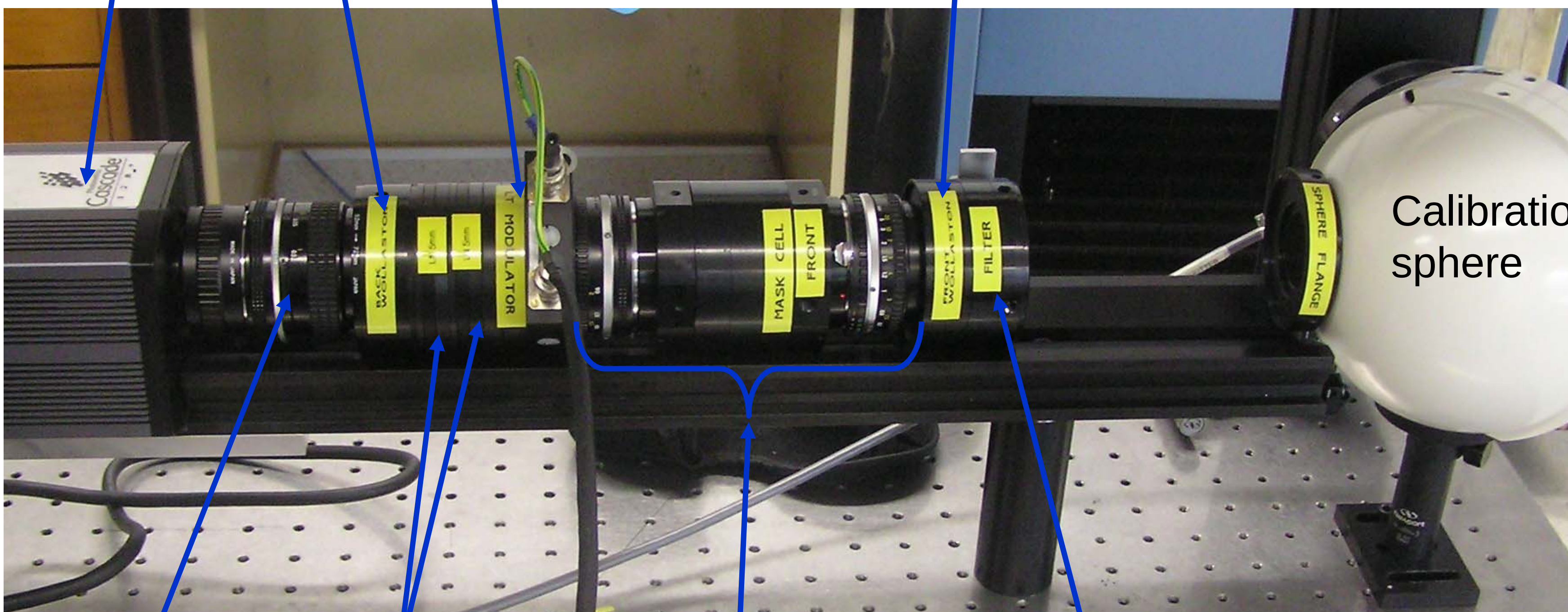

Calibration sphere

Imaging lens

Field-widened Lithium niobate Delay plates

Quad cell: lens-mask-lens

Interference filter

Calibration using EO modulator

screensnap of image browser

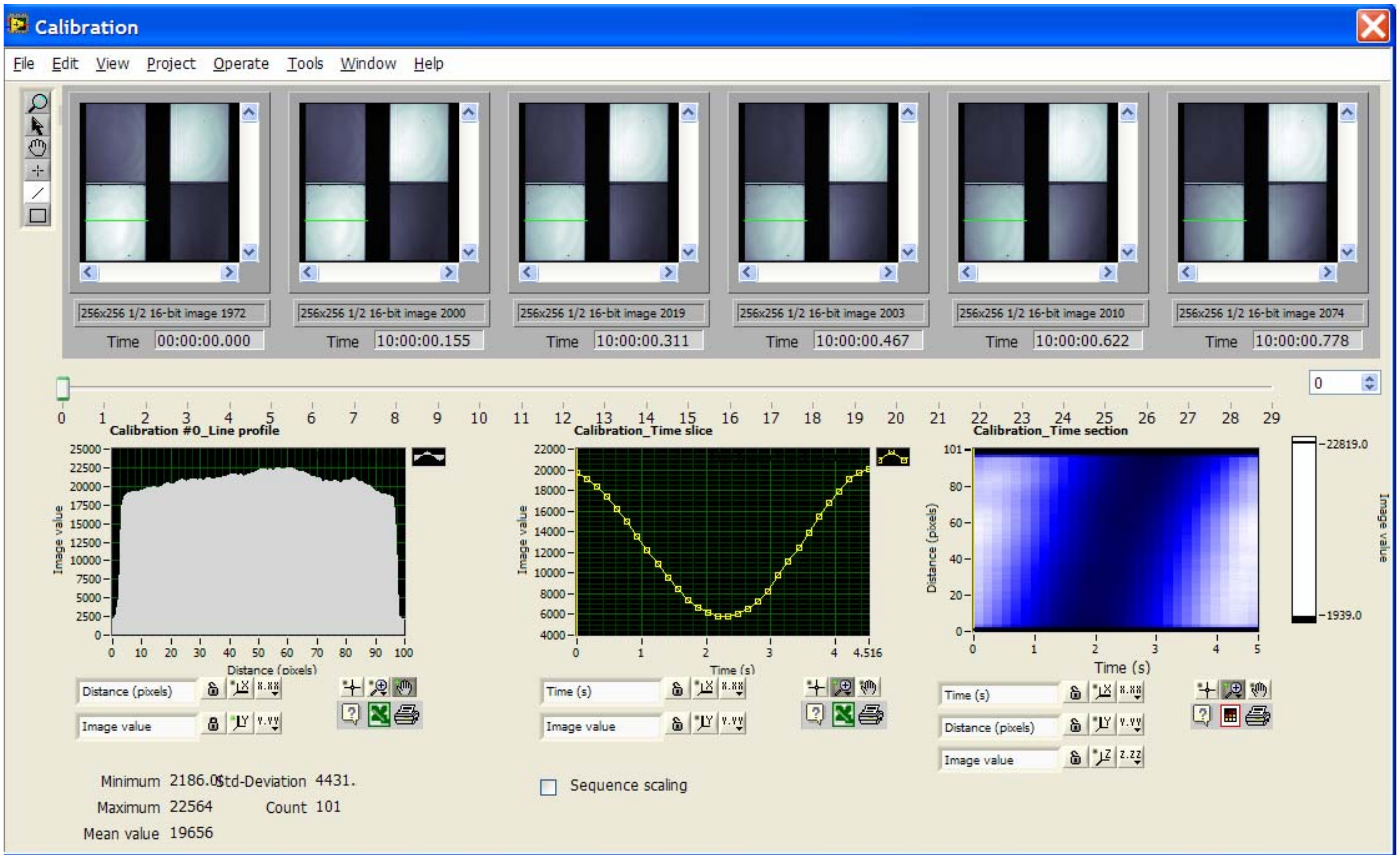

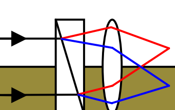

ANU

Calibration procedure and crosschecks

- Integrating sphere and lamp – diffuse monochromatic source
- Electrooptically ramp delay through ~1 wave and acquire image sequence
  - Zero-nett-delay lithium tantalate modulator
  - For each image point in the sequence, fit a sinewave to obtain intensity, contrast, phase
  - Non-EO calibration scheme is possible
- Spatially register the 4 quadrant images $S = I_0[1 + \zeta_i \cos \phi_i]$

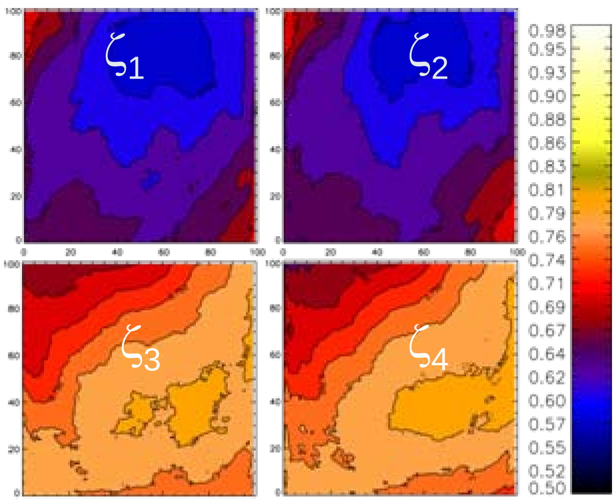

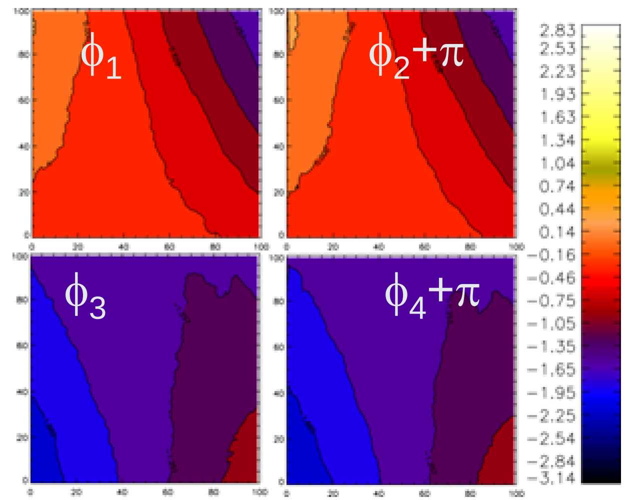

Instrument contrast images ζ_i
Left and right images should have same fringe contrast

Instrument phase images ϕ_i
Left and right images should be in antiphase

Degree of orthogonality between images determines condition of demodulation

Recovery of coherence information requires division by the quantity

$$\Delta = \zeta_1 \cos\phi_1 \, \zeta_2 \sin\phi_2 - \zeta_1 \sin\phi_1 \, \zeta_2 \cos\phi_2$$

ζ_1, ζ_2 are instrument contrasts (1, 2 denote upper and lower pairs)
ϕ_1, ϕ_2 are instrument phases
When images are in true quadrature $\Delta = 1$

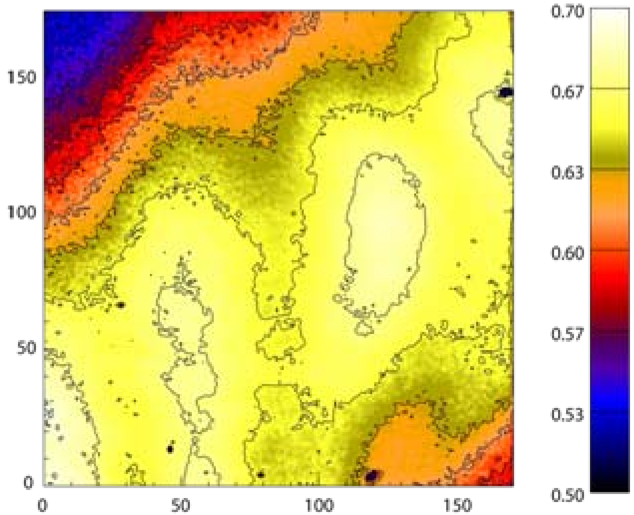

Contour map of Δ

Non-ideal due to

1. Design wavelength 529nm, observed 488nm
2. Imperfections in quarter wave plate manufacture

View through the H-1 vacuum port

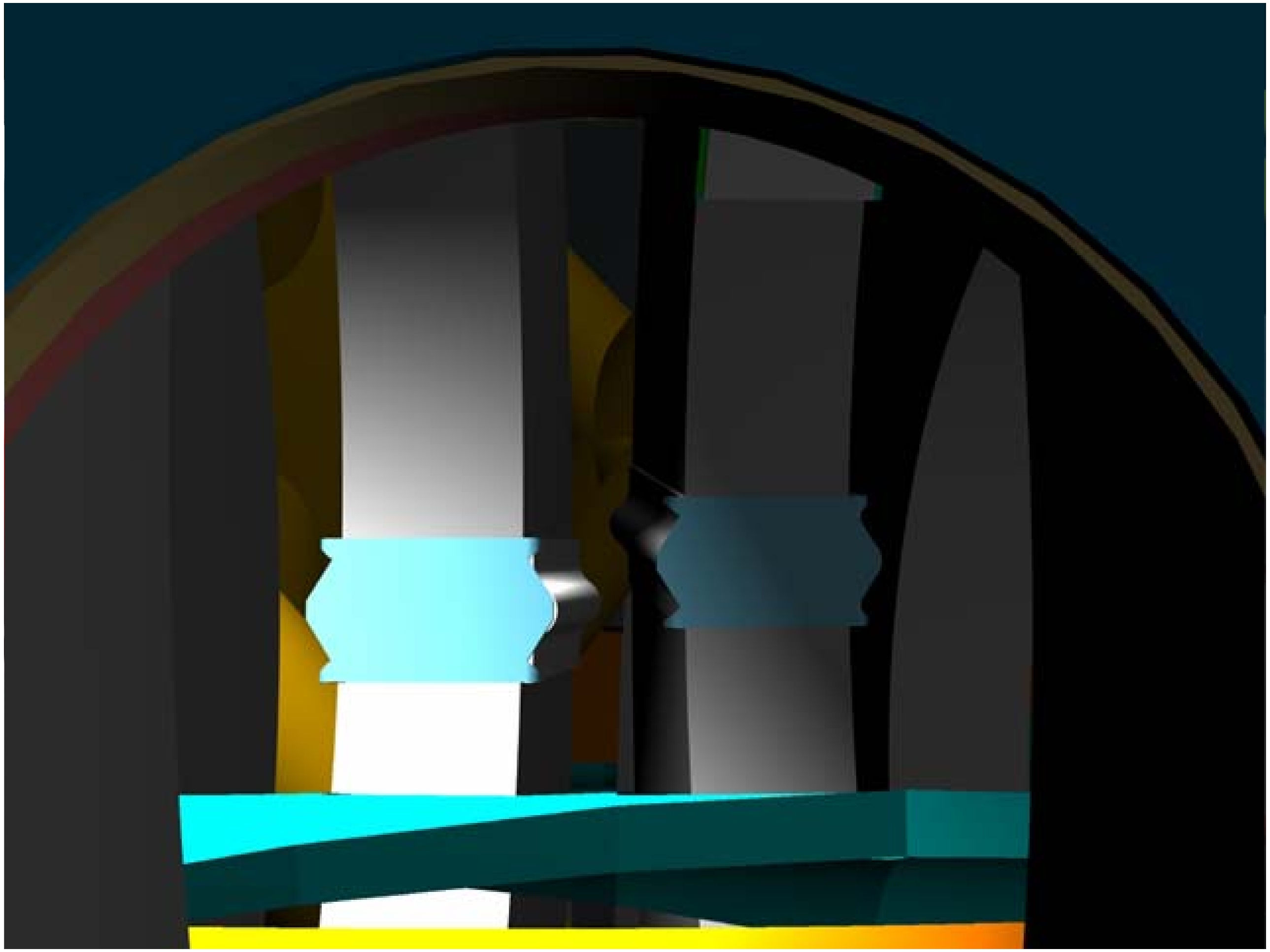

Raw quadrant coherence image data

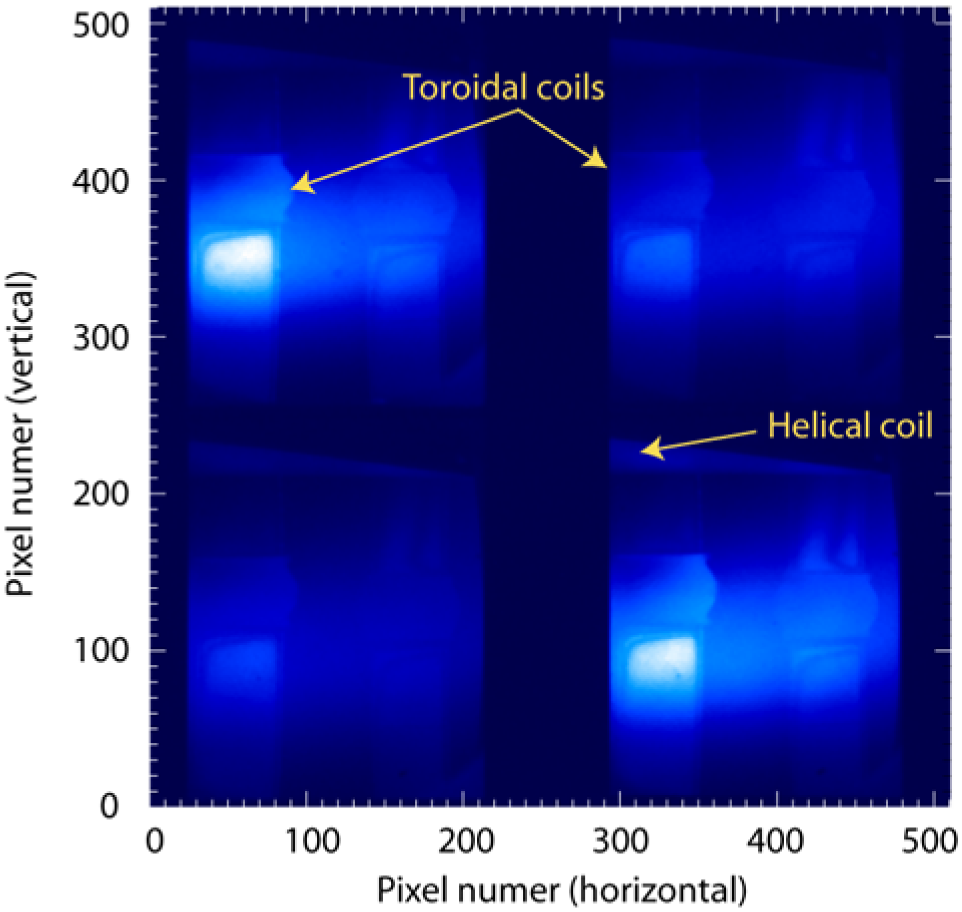

Cascade512 CCD camera
Image size 256x256
Exposure time/readout 8ms

Image size 512x512
Exp/readout 40ms

L-R separated images are anti-phase interferograms

Top-Bottom image pairs are in approximate quadrature

Individual images are inverted

Plasma behaviour at 0.12T

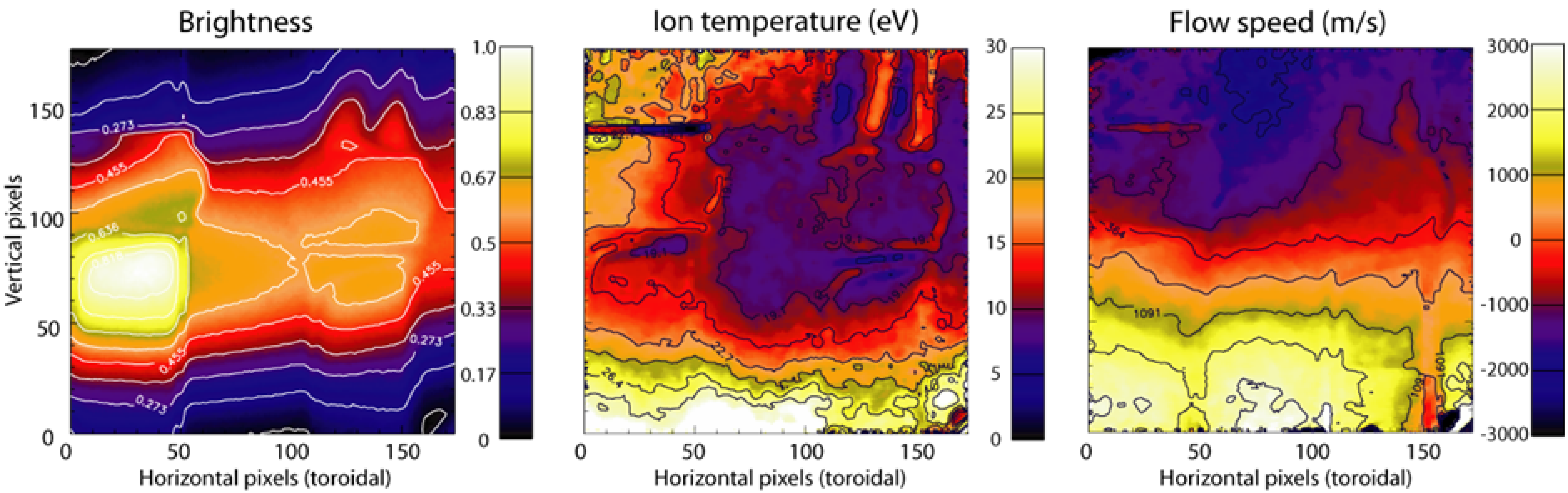

Brightness, temperature and flow images well decoupled

Hollow ion temperature and rigid rotation agrees with modulated 16-channel system

Ion temperature is invalid in region of reflection from coil surfaces

Registration artifacts evident

Plasma profiles at different optical delays

30mm (Tc=24eV) and 40mm (Tc=13eV) LN delay plates

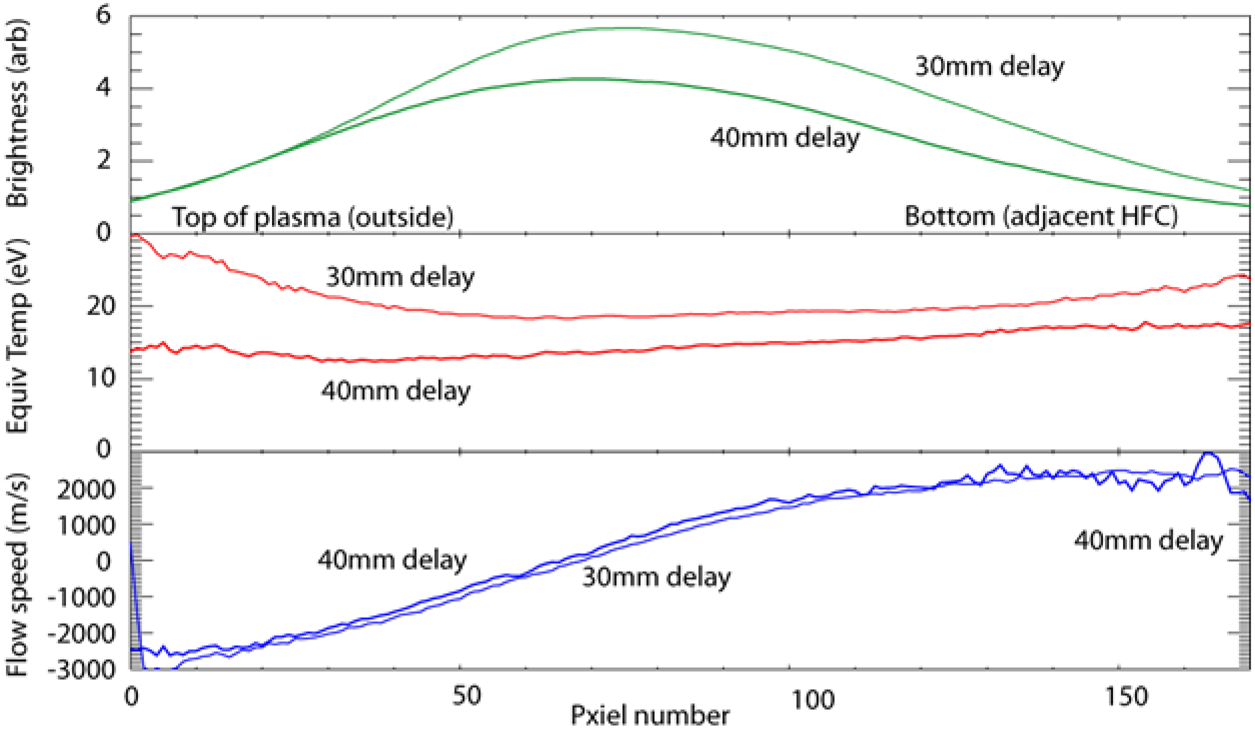

Average over 30-pixel wide region between toroidal field coils
Flow profiles identical
Inferred temperatures – discrepancy due to non-thermal distribution

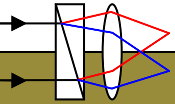

ANU

Conclusion and next step

- Fixed-delay coherence domain systems offer some advantages when the spectral information content is small
- Single delay modulated and static coherence imaging systems have application in
  - Doppler spectroscopy, Stark
  - Polarization spectroscopy (e.g. MSE)
  - Isotope concentration (Divertor, fuelling, H/D/T)
  - Broadband spectroscopy (Thomson, thermography ..)
- Hybrid temporal/spatial multiplex, multiple delay imaging systems can be used for more complex spectra
- Development of fast quadrature coherence system for imaging flow and temperature fluctuations.